SPE 106228

Adaptive Multiscale Streamline Simulation and Inversion for High-Resolution Geomodels

V. R. Stenerud, SPE, Norwegian U. of Science and Technology; V. Kippe, SINTEF ICT; A. Datta-Gupta, SPE, Texas A&M U.; and K.-A. Lie, SINTEF ICT.

This paper was prepared for presentation at the 2007 SPE Reservoir Simulation Symposium held in Houston, Texas, U.S.A., 26–28 February 2007.

Abstract

A particularly efficient flow solver can be obtained by combining a recent mixed multiscale finite-element method for computing pressure and velocity fields with a streamline method for computing fluid transport. This multiscale-streamline method has shown to be a promising approach for fast flow simulations on high-resolution geologic models with multimillion grid cells. The multiscale method solves the pressure equation on a coarse grid while preserving important fine-scale details. Fine-scale heterogeneity is accounted for through a set of generalized, heterogeneous basis functions that are computed numerically by solving local flow problems. When included in the coarse-grid equations, the basis functions ensure that the global equations are consistent with the local properties of the underlying differential operators. The multiscale method offers a substantial gain in computation speed, without significant loss of accuracy, when the multiscale basis functions are updated infrequently throughout a dynamics simulation.

In this paper we propose to combine the multiscale-streamline method with a recent 'generalized travel-time inversion' method to derive a fast and robust method for history matching high-resolution geologic models. A key point in the new method is the use of sensitivities that are calculated analytically along streamlines with little computational overhead. The sensitivities are used in the travel-time inversion formulation to give a robust quasilinear method that typically converges in a few iterations and generally avoids much of the subjective judgments and time-consuming trial-and-errors in manual history matching. Moreover, the sensitivities are used to control a procedure for adaptive updating of the basis functions only in areas with relatively large sensitivity to the production response. The sensitivity-based adaptive approach allows us to selectively update only a fraction of the total number of basis functions, which gives a substantial savings in computation time for the forward flow simulations.

We demonstrate the power and utility of our approach using a simple 2D model and a highly detailed 3D geomodel. The 3D simulation model consists of more than one million cells with 69 producing wells. Using our proposed approach, history matching over a period of 7 years is accomplished in less than forty minutes on an ordinary workstation PC.

Introduction

It is well known that geomodels derived from static data only – such as geological, seismic, well-log and core data – often fail to reproduce the production history. Reconciling geomodels to the dynamic response of the reservoir is critical for building reliable reservoir models. In the past few years, there have been significant developments in the area of dynamic data integration through the use of inverse modeling.[1-12] Streamline methods have shown great promise in this regard.[7-12] Streamline-based methods have the advantages that they are highly efficient "forward" simulators and allow sensitivities of production responses with respect to reservoir parameters to be computed analytically using a single flow simulation.[7-10] Sensitivities describe the change in production responses due to small perturbations in reservoir properties such as porosity and permeability and are a vital part of many dynamic data-integration processes.

Our recent works on streamline-based integration of production data were based on so-called 'generalized travel time inversion'.[7,8] There are several advantages associated with travel-time inversion of production data. First, it is robust and computationally efficient. Unlike conventional 'amplitude' matching, which can be highly non-linear, it has been shown that the travel-time inversion has quasilinear properties.[7,13] As a result; the minimization proceeds rapidly even if the initial model is not close to the solution. Second, the travel time sensitivities are typically more uniform between wells compared to 'amplitude' sensitivities that tend to be localized near the wells. This prevents over-correction in the near-well regions.[13] Finally, in practical field applications, the production data are often characterized by multiple peaks (for example, tracer responses). Under such conditions, the travel-time inversion can prevent the solution from converging to secondary peaks in the production response.[7]

Even though streamline simulation provides fast forward simulation compared with a full finite-difference simulation in 3D, the forward simulation is still the most time-consuming part of the history-matching process. A streamline simulation consists of two steps that are repeated: (i) solution of a 3D pressure equation to compute flow velocities; and (ii) solution of 1D transport equations for evolving fluid compositions along representative sets of streamlines, followed by a mapping back to the underlying pressure grid. The first step is referred to as the pressure step or the pressure solve and is often the most time-consuming. Consequently, history matching and flow simulation are usually performed on upscaled reservoir-simulation models.[14] However, upscaling/downscaling may result in loss of important fine-scale information. Recently, several multiscale methods for solving the pressure equation have proven to be a promising alternative to standard upscaling, both with respect to accuracy and efficiency.[15-18] These multiscale methods are specially designed to perform well when the underlying parameters exhibit a multiscale structure; that is, when the parameter values span several orders of magnitude or the correlation lengths of the heterogeneity structures vary over several orders. Like standard upscaling methods, the multiscale methods compute coarse-scale pressure velocities by solving a reduced set of global flow equations on a coarsened grid. These coarse-scale equations are defined in terms of the solutions of a set of local, decoupled flow problems. However, unlike upscaling methods, which only preserve the local flow in an averaged sense, multiscale methods try to preserve the subscale variations of the flow by finding approximate solutions that contain the most relevant fine-scale information. As a result, multiscale methods give pressure and/or flow velocities on both the coarse grid and on the original fine grid.

Multiscale methods are primarily targeted at dynamic flow simulations, where the pressure needs to be computed repeatedly. Since the temporal changes in the variable coefficients in the pressure equation are typically moderate compared to the spatial variability, it is seldom necessary to recompute the local flow problems each time the pressure is updated. Each local flow problem is computed initially as part of a preprocessing step (that is embarrassingly simple to parallelize) and typically only updated if the local domain is swept by a strong front in the fluid compositions or the global flow pattern changes significantly due to shut-in of wells, infill drilling, well conversion, etc. Hence, a pressure update typically consists of recomputing a few local flow problems and then solving a global flow problem on the coarse grid. This means that one can obtain an approximate solution on the original grid at the cost of solving the same problem on a much coarser grid.

In this paper, we combine multiscale-streamline simulation and streamline-based history matching in one efficient approach. For the pressure equation in the forward model we will apply a method we refer to as 'the mixed multiscale finite-element method' (MsMFEM).[19,20] The method uses a two-grid approach consisting of a fine grid, on which the geomodel is given, and a coarse grid, on which the global flow problem is solved. The blocks in the coarse grid are given as connected collections of cells from the fine grid. For each pair of adjacent blocks in the coarse grid, a local flow problem is solved on the underlying fine grid to obtain basis functions that are incorporated into a global system of equations associated with the coarse grid. MsMFEM produces mass-conservative solutions both on the coarse grid and on the underlying fine grid, is flexible with respect to grid representation (geometry/topology), and has a rigorous mathematical framework.

For the history matching we use the generalized travel-time inversion method, which has previously been successfully applied to many field cases. Central in this method is the computation of analytic streamline sensitivities in terms of simple 1-D integrals along streamlines. The sensitivities can be computed using a single streamline simulation. The second novel idea in this paper is a strategy based on sensitivity thresholding for reducing the workload for the forward simulation and for the inversion process. Altogether, the analytic sensitivities are used for three purposes: (i) in the inversion method, (ii) to reduce the computational complexity of the forward simulations by reducing the number of local flow solves, and (iii) to reduce computational complexity of the inversion process.

The outline of our paper is as follows. First, we discuss the basic steps in our proposed approach and illustrate the history-matching procedure using a simple synthetic example. Second, we describe the multiscale-streamline flow simulation and the history-matching procedure. Third, we discuss and demonstrate the impact of selective sensitivity-based workload reduction. Finally, we present a high-resolution history-matching example to demonstrate the efficiency and the practical applicability of our method.

Background and Illustration of the Procedure

Streamline-based history matching or inverse modeling utilizes streamline-derived sensitivities to calibrate geomodels to dynamic data. The major steps involved in the proposed process are: (i) Multiscale-streamline flow simulation to compute production responses at the wells. (ii) Quantification of the mismatch between observed and computed production responses via a generalized travel time. An optimal 'travel-time shift' is computed by systematically shifting the computed production responses towards the observed data until the cross-correlation between the two is maximized.[8] (iii) Computation of streamline-based analytic sensitivities of the production responses (water-cuts) to reservoir parameters, specifically permeability. (iv) Updating of reservoir properties to match the production history via inverse modeling. We propose a sensitivity-based thresholding strategy to reduce the computational work for this step.

This four-step process is repeated until a satisfactory match in production data is obtained. To reduce the computational workload for the forward simulation, we propose to reuse basis functions in regions with low sensitivity to the production responses.

In the next sections we will discuss the details of the mathematical formulation behind the multiscale mixed finite-element formulation and the inversion method, and propose a sensitivity-based strategy for selective work reduction. However, for clarity of exposition, we first illustrate the history matching procedure using a 2-D synthetic example.

A Synthetic Example. This synthetic case (Case 1) involves reconstruction of a reference permeability distribution on a uniform 21×21 grid **(Fig. 1)**, based on the observed water-cut production history from a 9-spot pattern **(Fig. 2)**. For the forward simulation we apply the MsMFEM-streamline simulator (to be described below), with the 21×21 grid as the underlying fine grid. We construct a uniform coarse grid of dimension 7×7 so that each coarse-grid block consists of 3×3 subcells. **Figure 3** illustrates the two-grid approach for a slightly more general case with nonmatching blocks in the coarse grid. The multiscale simulator basically works as follows: For each pair of adjacent blocks in the coarse grid, a local flow problem is solved to obtain a local (multiscale) basis function associated with the corresponding internal face in the coarse grid (see **Fig. 4**). The local basis functions are then incorporated into a global system of equations defined on the coarse grid, which is solved to obtain coarse-grid fluxes. Fine-scale flow velocities are then obtained by multiplying the coarse-grid fluxes with the corresponding multiscale basis function and summing over all edges in the coarse grid.

The flow was described using quadratic relative permeability curves with an end-point mobility ratio of M=0.5. The water-cut responses obtained from a flow simulation of the reference permeability field are shown in **Fig. 2** (with 5% white noise added). We treat these as the observed data. Next, starting from a homogenous initial permeability field, we match the water-cut data via the generalized travel-time inversion. The permeability for each fine-grid cell is treated as an adjustable parameter for this example (a total of 441 parameters). A comparison of the initial and final match of the water-cuts is shown in **Fig. 2**. Overall, the match to the production data is quite satisfactory. **Figure 5** shows the reduction in time-shift and amplitude residual. The final permeability distribution is shown in **Fig. 1**. Clearly, the final permeability model captures the large-scale trends of the reference permeability field.

Mathematical Formulation

Multiscale Flow Simulation. An important aspect of the proposed history-matching algorithm is the use of a multiscale mixed finite-element method (MsMFEM) for the pressure equation. This method belongs to a family of multiscale finite-element methods, first introduced by Hou and Wu.[21] The basic idea of the methods is to construct special finite-element basis functions that are adaptive to the local properties of the elliptic differential operator. To ensure local mass conservation on the coarse and fine grid, Chen and Hou introduced a multiscale method based on a mixed finite-element discretization.[19] The method was later modified by Aarnes to ensure local mass conservation also for blocks containing source terms.[20] In the current paper, we use a slightly different formulation due to Aarnes and Lie.[22]

Governing Equations. We consider incompressible two-phase flow of oil and water in a non-deformable permeable medium. For simplicity, we neglect the effects of gravity, compressibility and capillary forces. Further, we also assume for simplicity no-flow boundary conditions for the reservoir. The flow equations can be formulated as an elliptic equation for the pressure p and the total velocity v,

$$v = -\lambda_t k \nabla p, \quad \nabla \cdot v = q. \qquad (1)$$

Here q is a source term representing injection and production wells, k is the absolute permeability, and $\lambda_t = \lambda_t(S_w)$ is the total mobility. We will solve **Eq. 1** for the fine-scale velocity field v using MsMFEM, for which the details will be described in the next subsections.

The velocity field is used to obtain a streamline distribution. Along each streamline the 3D transport equation reduces to a 1D transport equation with the time-of-flight as the spatial coordinate

$$\frac{\partial S_w}{\partial t} + \frac{\partial f_w(S_w)}{\partial \tau} = 0. \qquad (2)$$

This equation is solved forward in time along each streamline using front tracking.[23,24] Here the main advantage of this method is that it is unconditionally stable and therefore avoids the usual CFL-constraint that would have put a severe limitation on the time-step size (i.e., enforce the time step to be smaller than what is preferred with respect to accuracy).

Mixed Finite Elements. The mixed finite-element formulation of the flow equation (**Eq. 1**) in a domain Ω seeks a pair (v,p) in $U \times V$, such that

$$\int_\Omega v \cdot (\lambda k)^{-1} u \, dx - \int_\Omega p \nabla \cdot u \, dx = 0, \qquad \forall u \in U, \qquad (3)$$

$$\int_\Omega l \nabla \cdot v \, dx = \int_\Omega q l \, dx, \quad \forall l \in V. \qquad (4)$$

Here U and V are (finite-dimensional) function spaces for pressure and velocity, respectively. Now, letting $\{\Psi_i\}$ and $\{\Phi_k\}$ be bases for U and V, respectively, we obtain approximations $v = \Sigma v_i \Psi_i$ and $p = \Sigma p_k \Phi_k$, where the coefficients $\mathbf{v} = \{v_i\}$ and $\mathbf{p} = \{p_k\}$ solve a linear system of the form

$$\begin{bmatrix} \mathbf{B} & \mathbf{C} \\ \mathbf{C}^T & \mathbf{0} \end{bmatrix} \begin{bmatrix} \mathbf{v} \\ -\mathbf{p} \end{bmatrix} = \begin{bmatrix} \mathbf{0} \\ \mathbf{q} \end{bmatrix}, \qquad (5)$$

where $\boldsymbol{B} = \{b_{ij}\}$, $\boldsymbol{C} = \{c_{ij}\}$ and $\boldsymbol{q} = \{q_k\}$ are defined by

$$b_{ij} = \int_\Omega \Psi_i \cdot (\lambda k)^{-1} \Psi_j \, dx, \qquad (6)$$

$$c_{ik} = \int_\Omega \Phi_k \nabla \cdot \Psi_i \, dx, \qquad (7)$$

$$q_k = \int_\Omega \Phi_k q \, dx. \qquad (8)$$

Multiscale Basis Functions. In a standard discretization, the spaces U and V typically consist of low-order piecewise polynomials. In multiscale methods, U and V are given by the solution of local flow problems. For incompressible flows, the actual pressure solution is immaterial for the flow simulation, and so only the velocity field is needed. We will therefore only construct an accurate multiscale approximation space U^{ms} for the velocity and use a standard approximation space V for pressure consisting of piecewise constant functions.

Let $\{K_m\}$ be a partitioning of Ω into mutually disjoint (fine) grid cells. Furthermore, let $\{T_i\}$ be a coarse partitioning of Ω, in such a way that whenever $K_m \cap T_i \neq 0$, then $K_m \subset T_i$ (see

Fig. 3). Let Γ_{ij} denote the non-degenerate interfaces $\Gamma_{ij}=\partial T_i \cap \partial T_j$. For each Γ_{ij}, we assign a basis function Ψ_{ij} in U_{ms}, and for each T_i we assign a basis function Φ_{i} in V. The basis function Ψ_{ij} is obtained by forcing a unit flow from block T_i to T_j; that is, by solving a local flow problem in $\Omega_{ij}=T_i \cup T_j$

$$\Psi_{ij} = -\lambda_t k \nabla \Phi_{ij}, \quad \nabla \cdot \Psi_{ij} = \begin{cases} w_i(x), & x \in T_i, \\ -w_j(x), & x \in T_j, \end{cases} \quad \text{..... (9)}$$

with $\Psi \cdot n=0$ on the boundary of Ω_{ij}. To give a unit flow from T_i to T_j, the source terms $w_i(x)$ are normalized

$$w_i(x) = W_i(x) \cdot \left(\int_{T_i} W_i(\xi)\, d\xi \right)^{-1}. \quad \text{..... (10)}$$

To ensure a conservative approximation of v on the fine grid, we choose $W_i=q$ for coarse blocks containing a well.[20] For coarse blocks where q=0, we scale W_i according to the trace of the permeability tensor[25]; i.e., we use

$$W_i(x) = \begin{cases} \text{trace}(k(x)), & \text{if } q(x)|_{T_i} = 0, \\ q(x), & \text{otherwise.} \end{cases} \quad \text{..... (11)}$$

The local flow problems in **Eq. 9** can be solved numerically by any consistent and conservative method; here we use the standard two-point flux-approximation scheme. The corresponding basis functions can be seen as generalizations of the lowest-order Raviart-Thomas basis functions in a standard mixed method.[26] **Figure 4** illustrates the x-velocity basis functions in two different cases. This completes the definition of MsMFEM.

Implementation of the MsMFEM. We will briefly describe some implementation aspects related to the efficiency and generality of MsMFEM. The mixed formulation leads to an indefinite global system (**Eq. 5**), which may be more difficult to solve efficiently than the symmetric positive-definite (SPD) systems that typically arise from standard discretization methods. However, by reformulating **Eq. 3** and **Eq. 4** to an equivalent, so-called hybrid, formulation, it is possible to obtain an SPD system also for MsMFEM. Like the indefinite system in **Eq. 5**, the hybrid system will be sparse because the basis functions have local support, and the solution can be obtained using one of the efficient linear solvers specialized for sparse SPD systems. The hybrid formulation is described in more detail by Aarnes et al.[27] We note that in our current implementation, we solve the global system in **Eq. 5** using a direct sparse solver, since we only deal with moderately sized coarse systems.

Most of the computational work in MsMFEM is associated with solving the local flow problems defined by **Eqs. 9 to 11**, and the choice of solution strategy for these equations is crucial to the overall performance of the method. The local problems are usually small to moderately sized, and the resulting systems can be solved using sparse direct or sparse iterative linear solvers. The optimal choice of linear solver typically depends on the problem size, and we recommend having available a range of solvers tuned to different system sizes. Alternatively, if one has access to a highly efficient solver for large sparse systems, it may be beneficial to lump together several local problems to form a larger system. Solving larger systems may be advantageous because the most efficient linear solvers typically require an initial setup phase. Regardless choice of solution strategy, efficient parallelization is easy, since the local flow problems are completely decoupled.

In the examples presented in this paper, we only use Cartesian grids. However, MsMFEM is flexible with respect to the choice of both fine and coarse grids. Given a fine-grid solver, basis functions can be defined for almost any collection of connected fine-grid cells.[25] Recently, the method has been implemented for (matching) corner-point and tetrahedral grids in 3D[27], and based on this experience we are confident that the methodology presented in the current paper is easily extended to corner-point grid models.

Production-Data Integration. In our approach, integration of production data is carried out using a 'generalized travel-time inversion' as described by He et al.[8] First, the production-data mismatch is determined by computing a 'generalized travel-time misfit' for the water-cut at each producing well. This is accomplished by shifting the computed water-cuts towards the observed data until the correlation between the two is maximized. The inversion algorithm simultaneously minimizes the travel-time misfit for all the wells using an iterative least-square minimization algorithm (LSQR).[7,8] The basic underlying principles behind the history-matching algorithm are briefly as follows:

- Match the field-production history within a specified tolerance. This is accomplished by minimizing the travel-time misfit for water-cut.
- Preserve geological realism by keeping changes to the prior geological model minimal, if possible. The prior model already incorporates static data (well and seismic data) and available geological information.
- Only allow for smooth and large-scale changes; the production data has low resolution and cannot be used to infer small-scale variations in reservoir properties.

Formulation of Inverse Problem. Mathematically, this algorithm leads to the minimization of a penalized misfit function consisting of the following three terms[7,8]**:**

$$\left\| \Delta \tilde{\mathbf{t}} - \mathbf{S}\delta\mathbf{m} \right\| + \beta_1 \left\| \delta\mathbf{m} \right\| + \beta_2 \left\| \mathbf{L}\delta\mathbf{m} \right\| \quad \text{.....(12)}$$

Here $\Delta\tilde{\mathbf{t}}$ is the vector of generalized travel-time shifts at the wells, $\mathbf{S}$ is the sensitivity matrix containing the sensitivities of the generalized travel time with respect to the reservoir parameters, $\delta\mathbf{m}$ corresponds to the changes in the reservoir properties, and $\mathbf{L}$ is a second-order spatial difference operator. The first term ensures that the difference between the observed and calculated production response is minimized. The two remaining terms are standard regularization terms. The second term is a norm constraint that penalizes deviations from the initial (prior) geological model and as such helps to preserve the geological realism in the history match. The third term, which is a 'roughness' constraint that measures the regularity of the changes, is introduced to stabilize the inversion. Physically, it only allows for large-scale changes that are consistent with the low resolution of the production data. The

weights β_1 and β_2 determine the relative strengths of the prior model and the roughness term.

The minimum in **Eq. 12** can be obtained by an iterative least-squares solution to the augmented linear system

$$\begin{pmatrix} \mathbf{S} \\ \beta_1 \mathbf{I} \\ \beta_2 \mathbf{L} \end{pmatrix} \delta\mathbf{m} = \begin{pmatrix} \Delta\tilde{\mathbf{t}} \\ \mathbf{0} \\ \mathbf{0} \end{pmatrix}. \quad \text{(13)}$$

This system is solved with the iterative least-square minimization algorithm, LSQR,[28] for which the computational cost scales linearly with respect to the number of degrees-of-freedom.[29] Fine-grid sensitivities close to zero are eliminated, which makes the system more sparse and reduces the number of arithmetic operations for the LSQR-iterations. In the next section we will discuss an approach to further reduce the number of non-zero sensitivities based on thresholding of coarse-grid sensitivities.

In our implementations we focus on inverting water-cut data. However, the generalized travel-time inversion method has earlier been extended to compressible three-phase flow, so that water-cut and gas-oil-ratios are incorporated jointly.[10]

Water-Cut Sensitivities. A unique feature of streamline methods is that the parameter sensitivities can be computed using a single flow simulation, leading to very fast history-matching or inverse-modeling algorithms. Moreover, because the sensitivities are simple integrals along streamlines, the computation time scales very favorable with respect to the number of grid cells, thus making streamlines the preferred approach for history matching highly-detailed geological models.

For the sake of completeness, we finally briefly describe the streamline-based sensitivity calculations. The velocity of propagation for a given saturation contour S_w along a streamline will be given by,

$$\left.\frac{\partial \tau}{\partial t}\right|_{Sw} = \frac{df_w}{dS_w} \quad \text{(14)}$$

and the arrival time of the saturation front will be,

$$t_a = \tau \Big/ \frac{df_w}{dS_w} \quad \text{(15)}$$

We use the above relationship to compute the sensitivity of the arrival time of the saturation front based on the sensitivity of the time-of-flight.[7,8] Specifically, the sensitivity of the arrival time of the saturation front with respect to reservoir parameter m is computed as,

$$\frac{\partial t_a}{\partial m} = \frac{\dfrac{\partial \tau}{\partial m}}{\dfrac{df_w}{dS_w}}. \quad \text{(16)}$$

Here the sensitivity of the time-of-flight is computed analytically from a single streamline simulation under the assumption that the streamlines do not shift because of small perturbations in reservoir properties. For example, the time-of-flight sensitivity with respect to permeability in grid cell i, under the assumption of the same permeability for the whole grid cell, will be given by[7]

$$\frac{\partial \tau}{\partial k_i} = \frac{\partial \tau_i}{\partial k_i} = \int_{\Sigma_i} \frac{\partial s(\xi)}{\partial k_i} d\xi = -\int_{\Sigma_i} \frac{s(\xi)}{k_i} d\xi = -\frac{\tau_i}{k_i}, \quad \text{(17)}$$

where the integral is along the streamline trajectory Σ and $s(x)$ is the 'slowness' defined as the reciprocal of the total interstitial velocity

$$s(x) = \frac{\phi(x)}{|v(x)|} = \frac{\mu\,\phi(x)}{k(x)|\nabla P|}. \quad \text{(18)}$$

Similarly, the time-of-flight sensitivities can be calculated with respect to mobility or to the product of mobility and permeability.

Finally, the sensitivity of the shift in the generalized travel time $\Delta\tilde{\mathbf{t}}$ with respect to reservoir parameters is given by

$$\frac{\partial \Delta\tilde{\tau}}{\partial m} = -\frac{1}{N_d} \sum_{a=1}^{N_d} \frac{\partial t_a}{\partial m}, \quad \text{(19)}$$

where N_d represents the number of observed data for a well.

Finally, we remark that the streamline-based sensitivity computation has been extended to include gravity, changing field conditions, and fractured reservoirs.[8,9]

Sensitivity-Based Selective Work Reduction

In this section, we discuss how the sensitivities introduced above can be used to reduce the computational complexity of the history matching with negligible loss in quality of the derived match. To this end, we use sensitivities to determine when to update and when to not update basis functions. Similarly, we will reduce the inverse system by only including the sensitivities of fine-grid cells within coarse blocks having a sufficiently high average sensitivity. These two strategies will be described in more detail below.

Selective Updating of Basis Functions. To reduce the computational work for MsMFEM, we propose to only update basis functions in areas with great production-response sensitivities. The inversion method provides sensitivities associated with the fine grid. To associate a sensitivity coefficient with each basis function, we compute the arithmetic average of fine-grid sensitivities over the domain where the basis function has support. To determine which basis functions to update, one can either: (i) use a predefined threshold for the sensitivity values, or (ii) update a predefined fraction of the basis functions. The first approach is fully adaptive in the sense that the number of updated basis functions may change from iteration to iteration. However, this approach requires (general) guidelines for setting the threshold, which may be easier to obtain by making the sensitivities dimensionless. The second approach requires sorting of the sensitivities. The number of basis functions is equal to the number of edges/faces, which scales with the number of coarse-grid blocks, and sorting them is therefore a minor concern, since the number of operations for sorting N numbers scales like $N \cdot \log N$. For our implementations we will stick to the second approach.

By inspecting **Eq. 9**, we notice that there are three factors that may require the basis functions to be updated before a new pressure solve. First of all, we notice that if the absolute

permeability k changes, the basis functions will change, too. In the current application, the absolute permeability will typically change (in certain regions) from one forward simulation to the next. Secondly, if the well rate q changes, the source term $w_i(x)$ will change and hence basis functions with support in well-blocks will change. Finally, if the total mobility λ_t changes, due to changes in saturation (or viscosities), the basis functions will change.

In the first flow simulation of the history-matching procedure, we update all basis functions in every pressure step, because no sensitivities are yet available. (In a more sophisticated implementation, one would typically have used another kind of indicator to ensure that basis functions are only updated near the saturation front[20,16]). After the first simulation, the permeability field is updated by the inversion method. Since the permeability field has changed, we should, at least in principle, recalculate all basis functions for the first pressure step of the next flow simulation. For the subsequent pressure steps of the simulation, we apply the proposed selective updating strategy. For the subsequent simulations we repeat the strategy of the second simulation. The approach described in this paragraph, when x% of the basis functions are updated dynamically each time step, is referred to as x% BF-DU (basis functions – dynamical update). Finally, we remark that for 0% BF-DU we will not update basis functions during the first flow simulation because no sensitivities are then required. This special case deviates from what we specified above.

An extended approach would be to reuse basis functions from the previous forward simulation in the coarse blocks where the absolute permeability has undergone small or no changes in the last inversion step. We suggest to use averaged production-response sensitivities to pick coarse blocks with small changes (or generally coarse blocks that have little effect on the overall production characteristics). Alternatively, one could use some kind of norm criteria to determine changes to the absolute permeability. We will refer to this strategy, where x% of the basis functions are updated initially and the remaining $(100-x)$% are kept from the previous flow simulation, as x% BF-IU (basis functions – initial update).

In the following, we will only use one of these two techniques at a time, although they may in principle be combined.

Selective Reduction of the Inversion System. Since the water-cut data contain limited information about fine-scale variations, it can be advantageous to avoid involving areas of low sensitivity in the inversion, and instead focus on resolving large-scale structures in areas with higher sensitivities. We therefore propose to eliminate fine-scale sensitivities from the LSQR-system (**Eq. 13**) in areas of low sensitivity, which will also reduce the computational work in the inversion process. To determine the areas of low and high sensitivity, we use a similar procedure as for the selective updating of basis functions. That is, for each coarse block we compute a sensitivity coefficient by arithmetic averaging of the fine-grid sensitivities already provided by the inversion method. Then we introduce a threshold and only include the fine-scale sensitivities associated with cells inside coarse blocks having an average sensitivity above the given threshold. The coarse blocks that are eliminated in this process will usually mainly contain cells with zero or low sensitivity.

The constraints involved in **Eq. 12** are important for the elimination of coarse blocks to work. As for the thresholding of basis functions, we can either use a predefined threshold for the sensitivity values or a predefined fraction of coarse blocks; here we use the second approach. Henceforth, keeping y% of the coarse blocks is referred to as y% CB. It should be noted that eliminating fine cells for a fraction of the coarse blocks having low sensitivity will not necessarily decrease the number of fine-grid sensitivities in the inverse system by the same fraction. The reason is cells with zero or small sensitivity are already eliminated, and such fine-grid sensitivities are more likely represented in coarse blocks with low sensitivity.

Impact of Selective Work Reduction

To investigate the accuracy of the proposed selective work reduction, we apply it to the synthetic 9-spot case presented earlier in this paper (Case 1). We will still refer to this case as Case 1 even though we will vary some parameters and strategies for selective work reduction.

First, we investigate the effect of the proposed strategy for selective dynamical updating of basis functions (BF-DU) for the forward simulation. To this end, we compare results obtained by updating 100%, 75%, 50%, and 25% of the basis functions, selected according to the associated coarse-grid sensitivity coefficients. (Here all basis functions are recomputed in the first step of each new forward simulation). **Table 1** shows the corresponding reductions for misfit in time-shift and amplitude after six iterations for an unfavorable mobility ratio (M=10) and two favorable mobility ratios (M=0.2 and M=0.5). In addition, the table reports the average discrepancy between the reference and derived permeability field measured by

$$\frac{1}{N}\sum_{i=1}^{N}|\log(k_i^{reference})-\log(k_i^{derived})| \quad \text{..... (20)}$$

Reductions in misfit for each iteration in the history-matching algorithm are shown in **Figs. 6** and **7** for M=10 and M=0.2, respectively. Similarly, some of the derived permeability fields from the history matches are shown in **Figs. 8** and **9**. In general, the data are well matched for all reduction strategies. However, since the inversion problem is ill-posed, a unique solution cannot be expected. Indeed the permeability fields obtained for the cases with unfavorable and favorable mobility ratios differ even when updating all basis functions.

Judging from **Fig. 8**, the derived permeability fields for the unfavorable mobility ratio do not seem to change much when reducing the number of dynamically updated basis functions. Following Aarnes[20], one can argue that it is in general quite safe to reduce the number of dynamically updated basis functions for unfavorable flow cases, since these are characterized by weak shocks and mostly smooth variations in the total mobility. For the favorable mobility ratio (M=0.2), the derived permeability fields seem to change more by reducing the fraction of basis functions updated. In this case, the flow will generally have strong saturation fronts, which induce major changes in the basis functions as the leading water fronts move through the corresponding grid blocks.

The above discussion is to a certain contradicted by the observed discrepancies in log(k), which show that derived permeability fields are actually (pointwise) closer to the reference field for M=0.2 than for M=10. Further, we observe a decreasing trend for the average discrepancies by reducing the number of basis functions that are dynamically updated for M<1, and conversely an increasing trend for M>1.

To further reduce the number of basis function computations we will try to apply the extended approach, in which we reuse basis functions from the previous forward simulation, for M=0.2, M=0.5 and M=10. We go directly to the extreme of keeping the basis functions from the first time step of the first flow simulations throughout the history-matching procedure. In other words, no updating of basis functions at all; that is 0% BF-DU and 0% BF-IU. The corresponding results are reported in **Table 1**, and **Fig. 10** shows the resulting permeability fields for mobility ratios M=0.2 and M=10. The quality of the history-matching procedure does not seem to decline dramatically by not updating basis functions at all for this case.

Finally, we investigate the effect of the proposed strategy for selective reduction of the inverse system. To this end, we consider the case with mobility ratios M=0.2, M=0.5 and M=10, and keep the fine-grid sensitivities corresponding to 100%, 75%, and 50% of the coarse-grid blocks, selected by thresholding the averaged sensitivities in the coarse grid. Keeping 100% for M=0.5 corresponds to the history matching performed for the 9-spot case initially in this paper. All the fractions matched the data well (see **Table 1** and **Fig. 11**). The derived permeability fields for M=0.5 for the three strategies 100% CB, 75% CB, and 50% CB are shown in **Figs. 1**, **12a,** and **12b**, respectively. The derived permeability fields do not change much when reducing the coarse-block fraction to 50%, but going down to 25% gave a non-realistic permeability field. We also note that for some cases, the selective reduction of the inverse system resulted in a slightly slower convergence for the inversion. The method converged to the same residual level as without selective work reduction, but the inversion required one or two additional iterations, thus resulting in increased total computation time. Even though the selective reduction of the inversion system can result in a slightly slower convergence, our experiments demonstrate robustness for the generalized travel-time inversion.

Finally we investigate the reduction strategy for the forward simulation (not extended approach) and the inversion simultaneously for the case with mobility ratios M=0.2, M=0.5 and M=10. We consider the combination of 50% BF-DU with 75% and 50% CB. The two cases matched the data well (see **Table 1** and **Fig. 11**). Further, the derived permeability fields for M=0.5 are shown in **Figs. 12c** and **12d**. The derived permeability fields do not change much by including selective updating of basis functions (see **Table 1**).

History Matching a Full 3D Geomodel

In this section we demonstrate the feasibility of the approach for field studies by application to a high-resolution 3-D example (Case 2). As mentioned before, streamlines and the time-of-flight are used to compute the sensitivity of the production data with respect to reservoir parameters as described above. In this field-scale example, water-cuts were matched to update the reservoir permeability distribution using the MsMFEM-streamline simulator for the forward simulation.

Model Description. The geomodel consists of a fine grid with 256×128×32 cells, which gives a total of 1,048,576 grid cells, each of size 10×10×2 m. The fine-grid cells are collected into a uniform 32×16×8 coarse grid, so that each coarse block consists of 8×8×4 cells in the fine grid. All the cells are treated as active.

The permeability is log-normally distributed with a mean of 2.2 mD, a minimum of 0.017 mD and a maximum of 79.5 mD (see **Fig. 13b**). The correlation length in the x- and y-directions is about 270 meters, and about 90 meters in the z-direction. For our purposes, this permeability field was used as a true or reference model to generate production history from flow simulation. To generate our reference production data we used the standard two-point flux-approximation (TPFA) finite-volume method directly on the fine grid.

A total number of 32 injectors and 69 producers were included in the simulation model (see **Fig. 14**). All the wells are vertical and intersect all layers. The production history consists of 2475 days of water-cut data from the 69 producers **(Fig. 15)**. The water injectors were injecting at constant total reservoir volume rate of 1609 STB/day, and each producer was producing with constant reservoir volume rate fulfilling the total voidage rate. For each simulation, we used 15 pressure steps of length 165 days. Further, quadratic relative permeability curves and end-point mobility ratio of M=5 were used.

Production Data Integration. To generate an initial permeability model, we treat the permeability values in the well-blocks of the reference model as known data. By conditioning on the well data, sequential Gaussian simulation was used to generate multiple realizations of the permeability model.[30]

In the following we will mainly consider three approaches: MsMFEM [full], MsMFEM [reduced] and TPFA. The two first approaches are multiscale approaches, while the last one simulates directly on the fine grid. Further, for the first and the last approach no selective work reduction occurs. For MsMFEM [reduced] the extended approach for reducing the number of basis function computations is applied. For each new forward simulation, the basis functions are sorted according to average sensitivities and for the lowest 50%, basis functions are kept from the previous flow simulation. For the remaining 50%, the basis functions are updated once before the first pressure solve. Moreover, selective reduction of the inverse system is used keeping fine-grid sensitivities for 50% of the coarse blocks. In other words:

- MsMFEM [full] = 100% DU + 100% IU + 100% CB,
- MsMFEM [reduced] = 0% DU + 50% IU + 50% CB.

Figure 16 and Table 2 show the convergence of the inversion algorithm. In six iterations, all misfits in time-shift and amplitude for the water-cut dropped appreciably for the three approaches. Reference, initial, and matched water-cut curves are shown in **Fig. 15** for a few selected producers. Some of the wells had a quite good match initially, and at the

end of the history matching all wells had a quite satisfactory match.

Figure 13 compares the initial and the reference permeability models with the updated (derived) models. The scale is logarithmic and the minimum permeability is 0.017 mD and the maximum is 112.3 mD. The three approaches gave almost identical derived permeability fields. Therefore, just one of the derived permeability fields (for MsMFEM [full]) is picked for closer inspections. From a casual look, it is hard to discern the changes made to the initial model. This is because the inversion algorithm is designed to preserve the geologic continuity and the initial geologic features to the maximum possible extent. However, a careful comparison reveals many differences between the initial and the updated geologic models.

Next, we examine if the changes made to the initial model are consistent with the 'reference' permeability model. **Figure 17** shows the differences between the updated and initial permeability model. These differences represent 'changes made'. This is to be compared with the 'changes needed', which is the difference between the reference and the initial permeability model. We see that there is clearly close agreement, particularly in regions where the permeability needs to be reduced (negative changes). As might be expected, there are also some discrepancies. Many of the wells had a good match initially even though the permeability fields differ. Because the water-cut data curves are a result of the total flow pattern between a producer and one or more injectors, this data source may have limited spatial information. Some of the changes occur in correct horizontal position, but incorrect vertical position. This can occur because the water-cut data has no vertical spatial resolution. Finally, it is worth pointing out that this inversion problem is highly ill-posed, and therefore a variety of possible solutions exist. **Table 2** shows average discrepancies between the reference and the derived permeability fields (see **Eq. 20**) for TPFA, MsMFEM [full], MsMFEM [reduced]. The average discrepancies indicate that the history-matching procedure is stable with respect to the selective work-reduction strategies. We have also investigated some other selective work-reduction strategies, and the results with respect to both misfit and average discrepancies turn out to be as stable as for Case 1.

To sum up, the changes made to the permeability field preserved the geologic realism, were mostly in accordance with the 'changes needed' (see **Fig. 17**), and resulted in satisfactory match of the water-cut data. Further, the different strategies for selective work-reduction turned out to give stable results with respect to 'changes made' and misfit (see **Table 2**).

Computational Efficiency. Finally, we will assess the efficiency of our multiscale method compared to a standard streamline method using a TPFA pressure solver. To this end, we consider two different computers running Linux: PC 1 is a laptop PC with a 1.7 GHz Intel Dothan Pentium M processor, 2Mb cache and 1.5 Gb memory, PC 2 is a workstation with a 2.4 GHz Intel Core 2 Duo, 4Mb cache, and 3 Gb memory.

Table 2 reports simulation times observed on the two computers. Here the total simulation time includes time for inversion, IO, and seven forward simulations, each with fifteen pressure steps. Similarly, we report the total time for the pressure solves and the transport solves (including mappings and tracing of streamlines).

When all basis functions are updated in all steps, the multiscale solver is, as expected, about 40% slower than TPFA with an optimal algebraic multigrid (AMG) solver on the laptop (PC1). On the other hand, the memory requirements for MsMFEM are quite low and this solver could easily have been run on larger models, as opposed to the TPFA methods, for which the AMG solver almost exceeded the available memory. Moreover, on highly skewed, non-Cartesian grids (e.g., corner-point grids), MsMFEM uses a much better spatial discretization[27] and will therefore give more accurate predictions of flow.

The comparison of TPFA and MsMFEM [full] is not very interesting on the workstation (PC2). Due to an immature compiler for the particular hardware, we were not able to optimize the direct solver used to compute basis functions, while the AMG solver could be (almost) fully optimized by using a vendor-specific compiler. The runtimes for the pressure solves (and the total runtime) on PC2 are therefore somewhat higher than expected, and will probably improve significantly when a more mature compiler becomes available in a few months.

By MsMFEM [reduced], we were able to reduce time for pressure solves by about 40% on both computers. In MsMFEM [reduced] the basis functions to be reused were read from file. Slow disc access on the laptop therefore prevented a further reduction in runtime. The workstation, on the other hand, had a faster disc, but further reductions in runtime were prevented by the unoptimized linear solver (as discussed above).

Reduction of the inverse system was expected to have a very small effect on the runtime, since a fully optimized compilation on a GHz processor gives a floating-point performance that would make the reduced number of arithmetic operations insignificant compared to other kinds of operations, which indeed is consistent with what we observe in **Table 2**. However, the results from the reduction of the inverse system indicate robustness for the generalized travel-time inversion method.

Finally, to speed the method further up, and to make our simulations comparable to state-of-the-art commercial streamline solvers, we apply a method for improved mass conservation for streamline simulation proposed by Kippe et al.[31] Using this method, the total number streamlines could be reduced from 500 000 to 50 000, thereby reducing the time for the transport solves by 80%. Altogether, this meant that the full history match could be performed in an impressive runtime of 39 minutes on the workstation (PC2) and 1 hour and 37 minutes on the laptop (PC1)!

For the workstation there is an obvious potential for further improvements by using a better compiler. Moreover, on Core 2 Duo processors one should also exploit the natural parallelism in updating basis functions and in the streamline computations. Finally, the total simulation time could easily be further reduced by removing unnecessary IO between the pressure solver and the inversion method.

Summary and Conclusions

A novel approach to history matching using multiscale-streamline simulation and analytic sensitivities is presented. The power and utility of our proposed approach is demonstrated using both a synthetic and a field-scale example. The synthetic case includes matching of water cut from a 9-spot pattern and is used to validate the method. The field-scale example consists of more than a million grid cells. Starting with a prior geomodel, production data were integrated using a generalized travel time inversion. The entire history matching process took about 1 hour and 40 minutes using a laptop PC and less than 40 minutes using an ordinary workstation PC. The permeability changes were found to be reasonable and geologically realistic.

Some specific conclusions from this paper can be summarized as follows.

1. A multiscale-streamline flow simulator was used for history matching by generalized travel-time inversion.
2. By utilizing the production-response sensitivities provided by the generalized travel-time inversion, we were able to reduce the total workload for the multiscale simulator considerably and still preserve the accuracy of the flow simulation.
3. By utilizing the production-response sensitivities, we were able to selectively reduce the number of non-zero sensitivities in the inverse system considerably without reducing the accuracy of the production data integration. This demonstrates robustness for the generalized travel-time inversion.
4. The approach proved applicable and efficient for a high-resolution reservoir model.

Acknowledgements

The research of Stenerud was funded by the *Uncertainty in Reservoir Evaluation (URE)* program at the Norwegian University of Science and Technology. The research of Kippe and Lie was funded by the Research Council of Norway under grant number 152731/S30. We wish to thank Dr. Yalchin Efendiev for helpful discussions.

Nomenclature

v = velocity
p = pressure
l,u = test functions
V,U = function spaces
K = fine grid cells/elements
T = coarse grid blocks/elements
Ω = domain
Γ = coarse block interface
n = unit normal vector
Ψ = basis function velocity
Φ = basis function pressure
q = total rate (source/sink)
f_w= fractional flow function (water)
S_w = saturation of water
k = absolute permeability
λ_t = total mobility
M = end-point mobility ratio
m = reservoir parameter
N_d= number of data points
N = number of grid cells

Subscripts

ms = multiscale

References

1. Anterion, F., Karcher, B., and Eymard, R. "Use of Parameter Gradients for Reservoir History Matching," paper SPE 18433 presented at the 1989 SPE Symposium on Reservoir Simulation, Houston 6-8 February.
2. Landa, J.L., Kamal, M.M., Jenkins, C.D., and Horne, R.N.: "Reservoir Characterization Constrained to Well Test Data: A Field Example," paper SPE 36511 presented the 1996 SPE Annual Technical Conference and Exhibition, Denver 6-9 October.
3. Wu, Z., Reynolds, A. C., and Oliver, D.S.: "Conditioning Geostatistical Models to Two-Phase Production Data," *SPE Journal* (June 1999) **4**(2), 142-155.
4. Oliver, D. S., Reynolds, A. C., Bi, Z., and Abacioglu, Y., "Integration of Production Data into Reservoir Models," *Petroleum Geoscience* (2001) **7**, S65-S73.
5. Reis, L.C., Hu, L.Y., and Eschard, R.: "Production Data Intergration Using a Gradual Deformation Approach: Application to an Oil Field (Offshore Brazil)," paper SPE 63064 presented at the 2000 Annual Technical Conference and Exhibition, Dallas, Texas, 1-4 October.
6. Sahni, I., and Horne, R.: "Multiresolution Wavelet Analysis for Improved Reservoir Description," *SPE Reservoir Evaluation & Engineering* (February 2005), 53-69.
7. Vasco, D.W., Yoon, S., and Datta-Gupta, A.: "Integrating Dynamic Data Into High-Resolution Models Using Streamline-Based Analytic Sensitivity Coefficients," *SPE Journal* (December 1999), 389-399.
8. He, Z., Datta-Gupta, A., and Yoon, S.: "Streamline-Based Production Data Integration with Gravity and Changing Field Conditions," *SPE Journal* (December 2002) **7**(4), 423-436.
9. Al-Harbi, M., Cheng, H., He, Zhong, and Datta-Gupta, A.: "Streamline-based Production Data Integration in Naturally Fractured Reservoirs," *SPE Journal* (December 2005), 426-439.
10. Cheng, H., Oyerinde, D., Datta-Gupta, A., and Milliken, W.: "Compressible Streamlines and Three-Phase History Matching," paper SPE 99465 presented at the 2006 SPE/DOE Symposium on Improved Oil Recovery, Tulsa, 22–26 April.
11. Milliken, W. J., Emanuel, A. S., and Chakravarty, A.: "Application of 3-D Streamline Simulation to Assist History Matching," paper SPE 63155 presented at the 2000 Annual Technical Conference and Exhibition, Dallas, Texas, 1-4 October.
12. Wang, Y., and Kovscek, A. R.: "A Streamline Approach to History Matching Production Data," *SPE Journal* (2000) **5**, 353-362.
13. Wu, Z., and Datta-Gupta, A.: "Rapid History Matching Using a Generalized Travel Time Inversion Method," *SPE Journal* (June 2002), 113-122.
14. Christie, M.A., and Blunt, M.J.: "Tenth SPE Comparative Solution Project: A Comparison of Upscaling Techniques", *SPE Reservoir Evaluation & Engineering* (August 2001), 308-317.

15. Gautier, Y., Blunt, M.J., and Christie, M.A.: "Nested Gridding and Streamline-Based Simulation for Fast Reservoir Performance Prediction," *Computational Geosciences* (1999) **3**, No. 3-4, 295-320.
16. Jenny, P., Lee, S.H., and Tchelepi, H.A.: "Adaptive Multiscale Finite-Volume Method for Multiphase Flow and Transport in Porous Media," *Multiscale Modeling and Simulation* (2004) **3**, No. 1, 50-64.
17. Arbogast, T., and Bryant, S. L.: "A Two-Scale Numerical Subgrid Technique for Waterflood Simulations," *SPE Journal* (December 2002), 446-457.
18. Aarnes, J.E., Kippe, V., and Lie, K.-A.: "Mixed Multiscale Finite Elements and Streamline Methods for Reservoir Simulation of Large Geomodels," *Advances in Water Resources* (2005) **28**, No. 3, 257-271.
19. Chen, A., and Hou, T.H.: "A Mixed Multiscale Finite Element Method for Elliptic Problems with Oscillating Coefficients," *Mathematics of Computation* (2002) **72**, No. 242, 541-576.
20. Aarnes, J.E.: "On the Use of a Mixed Multiscale Finite Element Method for Greater Flexibility and Increased Speed or Improved Accuracy in Reservoir Simulation," *Multiscale Modeling and Simulation* (2004) **2**, No. 3, 421-439.
21. Hou, T.Y. and Wu, X.-H.: "A Multiscale Finite Element Method for Elliptic Problems in Composite Materials and Porous Media," *Journal of Computational Physics* (1997) **134**, No. 1, 169-189.
22. Aarnes, J.E., and Lie, K.-A.: "Toward Reservoir Simulation on Geological Grid Models," *Proc.*, 9th European Conference on the Mathematics of Oil Recovery, Cannes, France, 30 August - 2 September, (2004), B21.
23. Bratvedt, F., Bratvedt, K., Buchholz, C.F., Holden, L., Holden. H., Risebro, N.H.: "A New Front-Tracking Method for Reservoir Simulation," *SPE Reservoir Engineering* (February 1992) 7, 107-116.
24. Holden, H., and Risebro, N.H.: *Front Tracking for Hyperbolic Conservation Laws*, Springer-Verlag New York Inc. (2002), ISBN 3-540-43289-2.
25. Aarnes, J.E., Krogstad, S., and Lie, K.-A.: "A Hierarchical Multiscale Method for Two-Phase Flow Based upon Mixed Finite Elements and Nonuniform Coarse Grids," *Multiscale Modeling and Simulation* (2006) **5**, No. 2, 337-363.
26. Raviart, P.-A., and Thomas, J.M.: "A Mixed Finite Element Method for 2nd Order Elliptic Problems", *Mathematical Aspects of Finite Element Methods (Proc. Conf., Consiglio Naz. Delle Ricerche (C.N.R), Rome, 1975)*, Lecture Notes in Mathematics, Springer, Berlin (1977) **606**, 292-315.
27. Aarnes, J.E., Krogstad, S., and Lie, K.-A.: "Multiscale Mixed/Mimetic Methods on Corner-Point Grids," *Computational Geosciences*, submitted.
28. Paige, C.C., and Saunders, M.A.: "LSQR: An Algoritm for Sparse Linear Equations and Sparse Least Squares," *ACM Transactions on Mathematical Software* (March 1982) 8, No. 1, 43.
29. Vega, L., Rojas, D., and Datta-Gupta, A.: "Scalability of the Deterministic and Bayesian Approaches to Production-Data Integration into Reservoir Models," *SPE Journal* (September 2004) 9(3), 330-338.
30. Deutsch, C.V., and Journal, A.G.: *GSLIB Geostatistical Software Library and User's Guide*, Oxford University, (1998).
31. Kippe, V., Hægland, H., and Lie, K.-A.: "A Method to Improve Mass Conservation in Streamline Methods", paper SPE106250 presented the SPE Annual Reservoir Simulation Symposium 2007, Houston, 26-28 February.

Table 1 – Case 1: Reduction in percent for misfit in time-shift (T) and amplitude (A), and reduction in average discrepancy in log permeability ($\Delta\log(k)$**). The results are presented for different strategies for selective work reduction and different mobility ratios *M*. The first row shows the results for the initial permeability field.**

Method			*M*=0.2			*M*=0.5			*M*=10		
DU	IU	CB	T	A	$\Delta\log(k)$	T	A	$\Delta\log(k)$	T	A	$\Delta\log(k)$
Initial			100.0	100.0	1.045	100.0	100.0	1.045	100.0	100.0	1.045
100%	100%	100%	6.0	13.5	0.636	5.7	13.4	0.640	6.1	23.0	0.739
75%	100%	100%	4.6	12.7	0.630	5.1	13.5	0.640	7.7	23.5	0.751
50%	100%	100%	3.3	12.6	0.609	5.5	13.6	0.613	6.5	23.7	0.763
25%	100%	100%	5.9	16.9	0.603	2.6	15.9	0.608	8.0	24.0	0.773
100%	100%	75%	5.6	13.2	0.610	4.9	13.0	0.614	7.2	23.0	0.690
100%	100%	50%	5.5	12.8	0.664	5.2	13.3	0.711	6.2	23.2	0.717
50%	100%	75%	3.1	12.4	0.577	3.8	13.3	0.571	6.0	23.6	0.702
50%	100%	50%	4.3	14.2	0.596	2.3	12.8	0.665	7.9	24.7	0.762
0%*	0%	100%	5.8	18.1	0.656	2.1	17.1	0.645	8.7	24.0	0.826

**Does not update basis functions during the first flow simulation*

Table 2 – Case 2: Reduction in percent for misfit in time-shift (T) and amplitude (A). Reduction in average discrepancy in log permeability (Δlog(k)). The total simulation time for the history-matching procedure for our implementations on two different computers: a 1.7GHz laptop (PC 1), and a 2.4GHz workstation (PC 2). The CPU-time for the two computers spent on the pressure (velocity) solutions and the transport solutions. The first row shows the results for the initial geomodel.

	T	A	Δlog(k)	Total simulation time (Wall clock)		Total CPU-time:			
						Pressure		Transport	
				PC1	PC2	PC1	PC2	PC1	PC2
Initial	100.0	100.0	0.821	-	-	-	-	-	-
TPFA	8.9	53.5	0.103	3h 09min	1h 12min	1h 27min	33min	1h 07min	29min
MsMFEM [full]	10.3	53.1	0.110	3h 29min	2h 50min	2h 01min	2h 08min	1h 00min	31min
MsMFEM [reduced]	7.8	53.7	0.113	2h 20min	1h 04min	52min	21min	1h 00min	32min
MsMFEM [reduced - SL]	7.6	48.7	0.124	1h 37min	39min	52min	21min	11min	6min

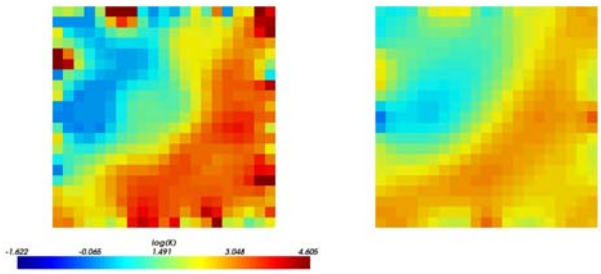

Fig. 1 – Case 1: Reference and final permeability fields (left and right, respectively) for mobility ratio M=0.5.

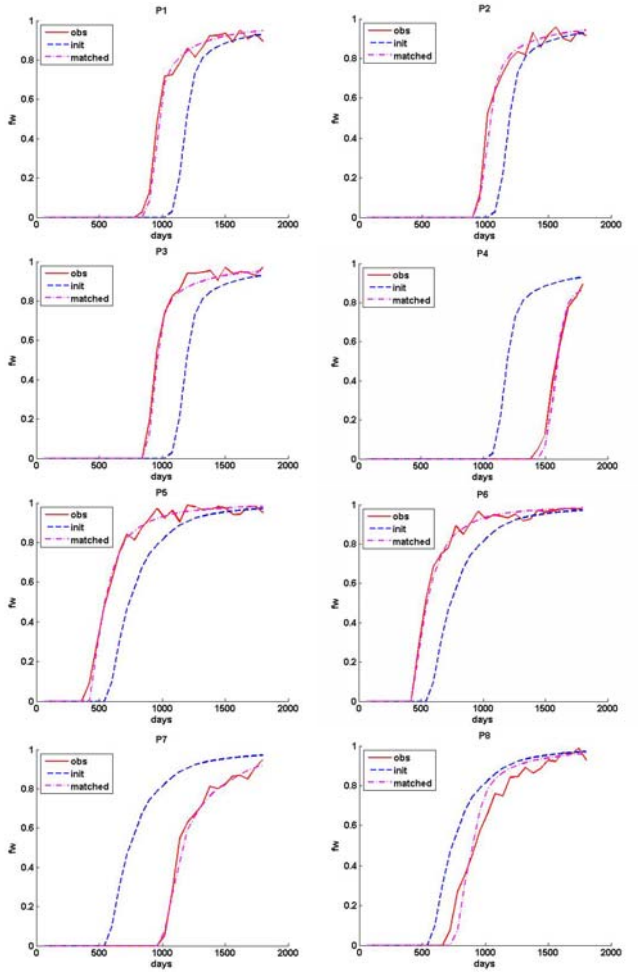

Fig. 2 - Case 1: water-cut match.

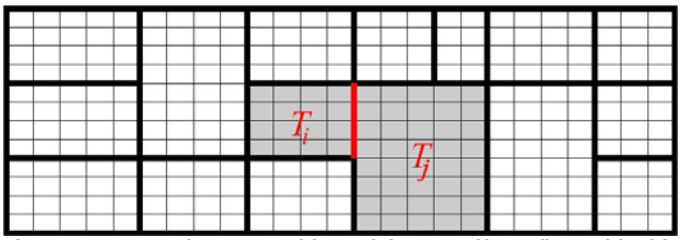

Fig. 3 - A general coarse grid overlying a uniform fine grid with the gray area giving support of basis function Ψ_{ij}, which is associated with the edge/face indicated by the red line.

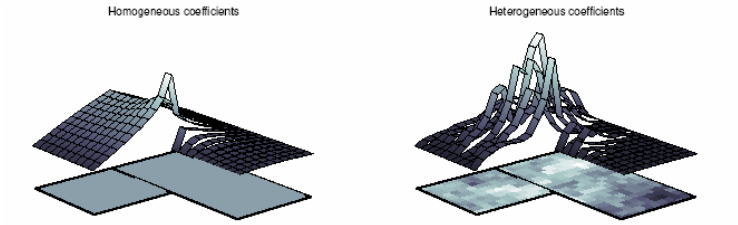

Fig. 4 -- The x-component of the velocity basis function associated with an edge/face between two blocks of different size for a homogeneous and a heterogeneous permeability field, respectively.

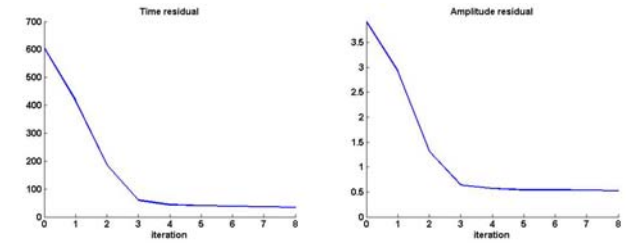

Fig. 5 – Case 1: Reduction of misfit in time-shift and amplitude of the water-cut. Mobility ratio M=0.5.

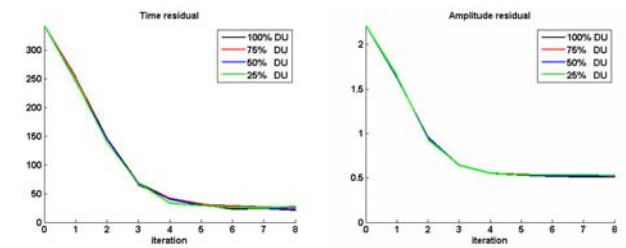

Fig. 6 – Case 1: Reduction of misfit in time-shift and amplitude of the water-cut using selective updating of basis functions.

Mobility ratio *M*=10.

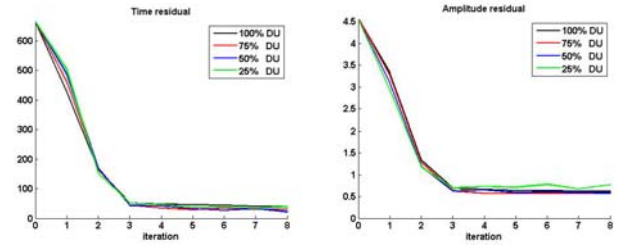

Fig. 7 – Case 1: Reduction of misfit in time-shift and amplitude of the water-cut using selective updating of basis functions. Mobility ratio *M*=0.2.

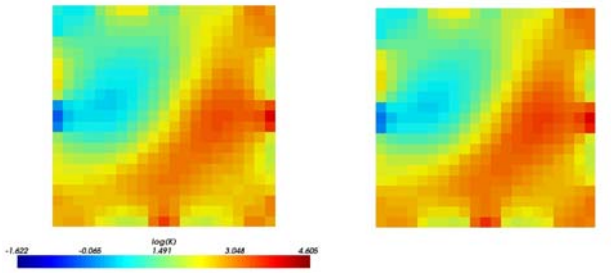

Fig. 8 – Case 1: Derived permeability field using selective updating of basis functions. Updating 100% (left) and 25% (right) of the basis functions. Mobility ratio *M*=10. The reference permeability field is shown in Fig. 3a.

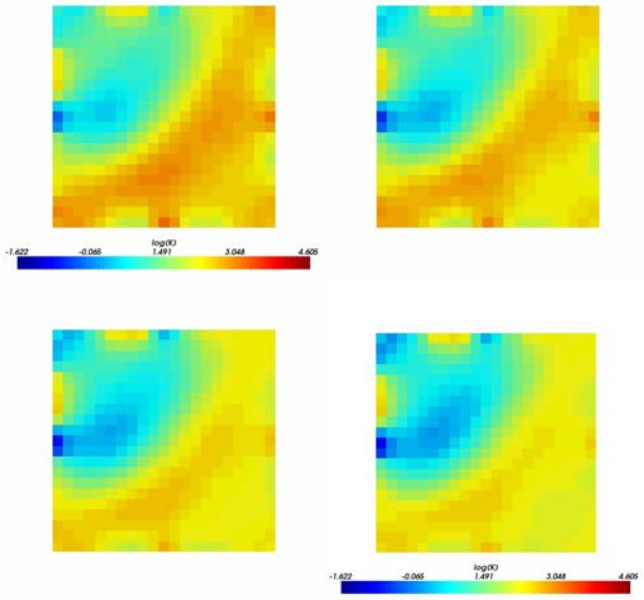

Fig. 9 – Case 1: Derived permeability field using selective updating of basis. Updating 100%, 75%, 50% and 25% of the basis functions (left to right from top), respectively. Mobility ratio *M*=0.2. The reference permeability field is shown in Fig. 3a.

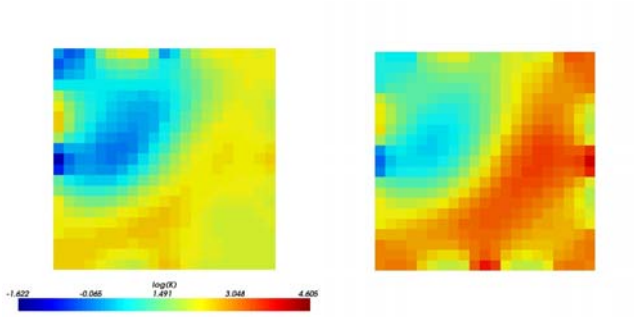

Fig. 10 – Case 1: Derived permeability field without updating basis functions throughout the history matching procedure for *M*=0.2 (left) and *M*=10 (right).

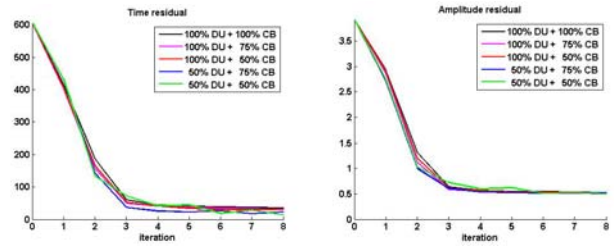

Fig. 11 – Case 1: Reduction of misfit in time-shift and amplitude of the water-cut using selective work reduction also for the inversion system. Mobility ratio *M*=0.5.

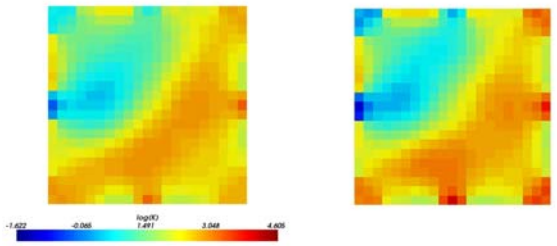

a) 100% DU + 75% CB **b) 100% DU + 50% CB**

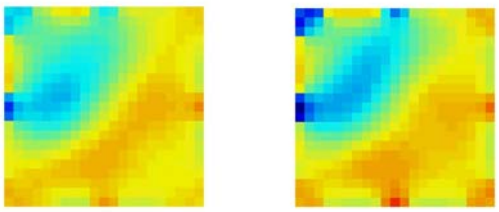

c) 50% DU + 75% CB **d) 50% DU + 50% CB**

Fig. 12 – Case 1: Derived permeability field using selective work reduction also for the inversion system. Mobility ratio *M*=0.5. The reference permeability field is shown in Fig. 3a.

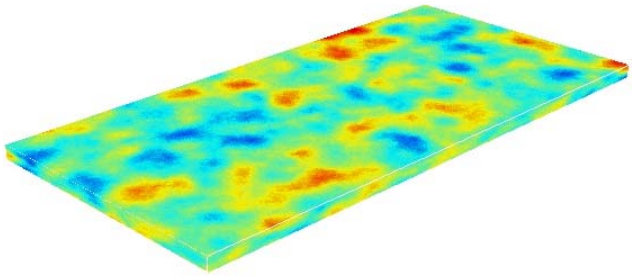

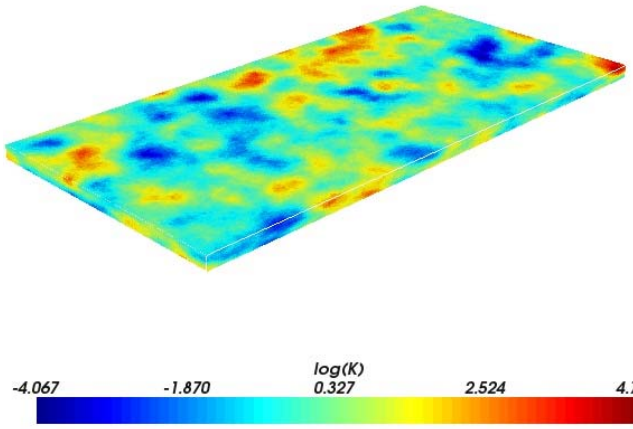

(a) Initial permeability (b) Reference permeability

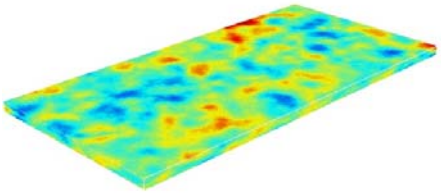

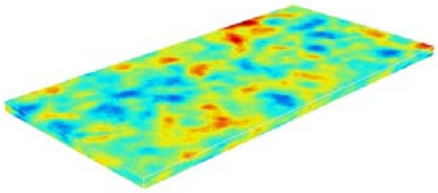

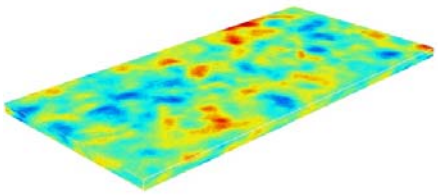

(c) Derived permeability (MsMFEM [full]) (d) Derived permeability (MsMFEM [reduced]) (e) Derived permeability (TPFA)

Fig. 13 – Case 2: Initial, derived and reference permeability fields.

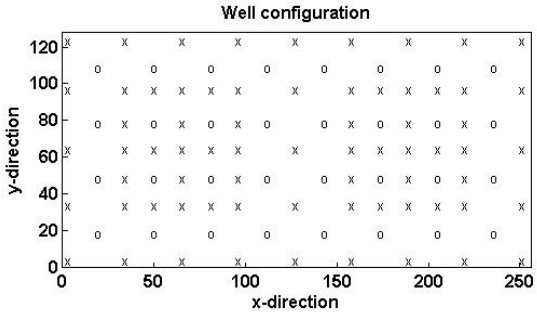

Fig. 14 – Case 2: Well configuration for the geologic model example. The symbol x represents a producer while the symbol o represents an injector.

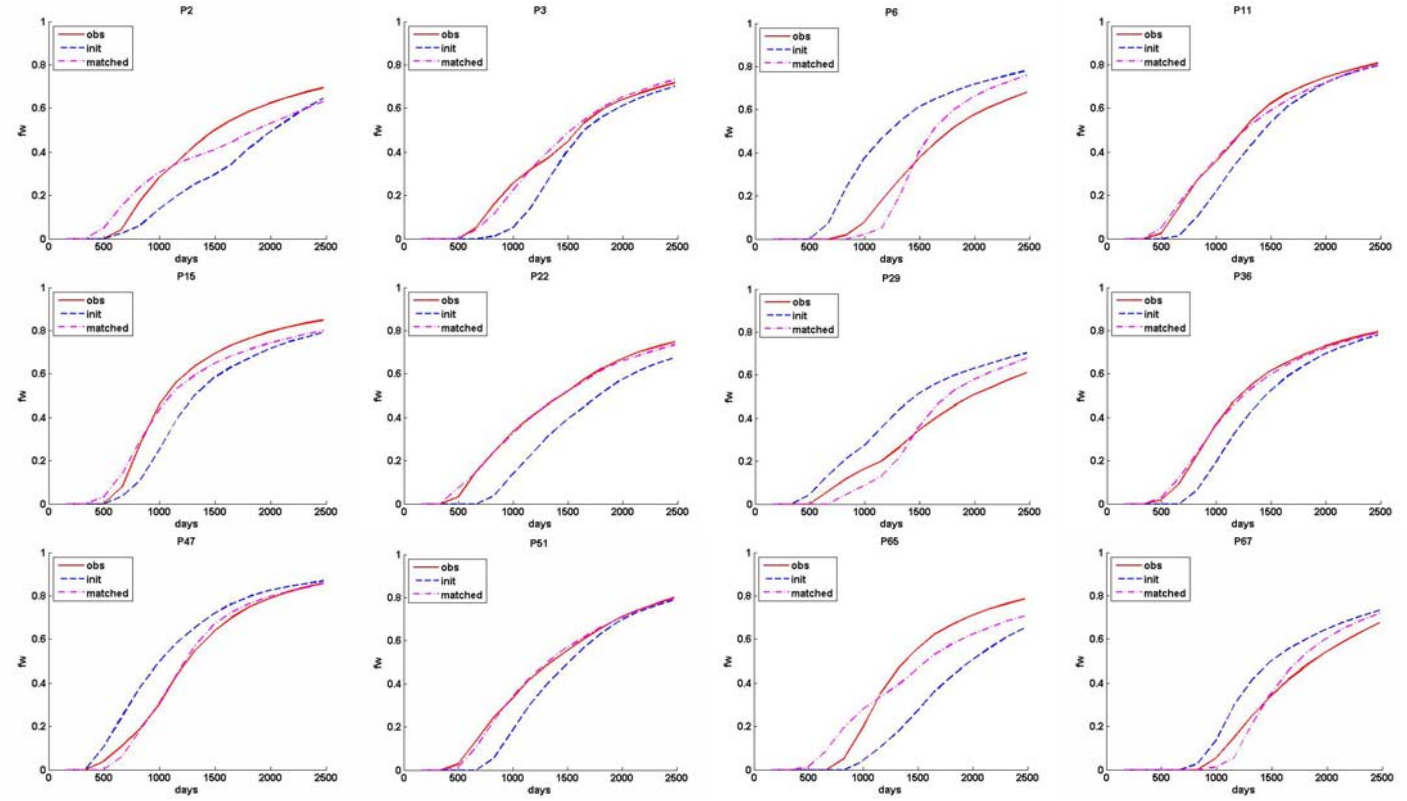

Fig. 15 – Case 2: Water-cut match for 12 of the 69 production wells included in the history match of the geologic model (MsMFEM [full]). For each plot the solid red line, the dash blue and the dashed purple line represents the reference, the initial and the updated water-cut curve, respectively.

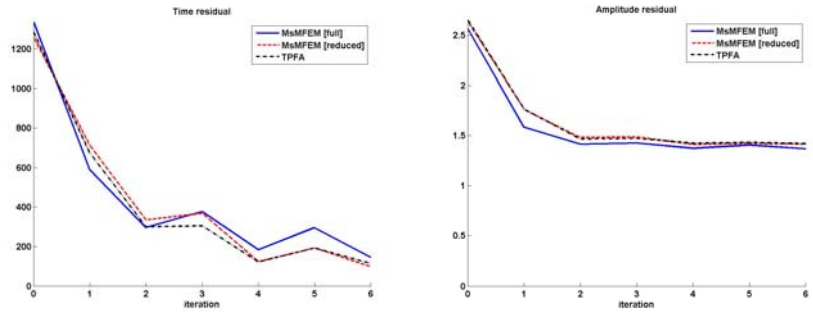

(a) Shift-time Misfit (days). **(b) Amplitude Misfit.**

Fig. 16 – Case 2: Reduction of misfit in time-shift and amplitude of the water-cut for history matching of geologic model. Forward simulation: MsMFEM [full] (blue solid curve), MsMFEM [reduced] (red dashed curve) and TPFA (black dash-dotted curve).

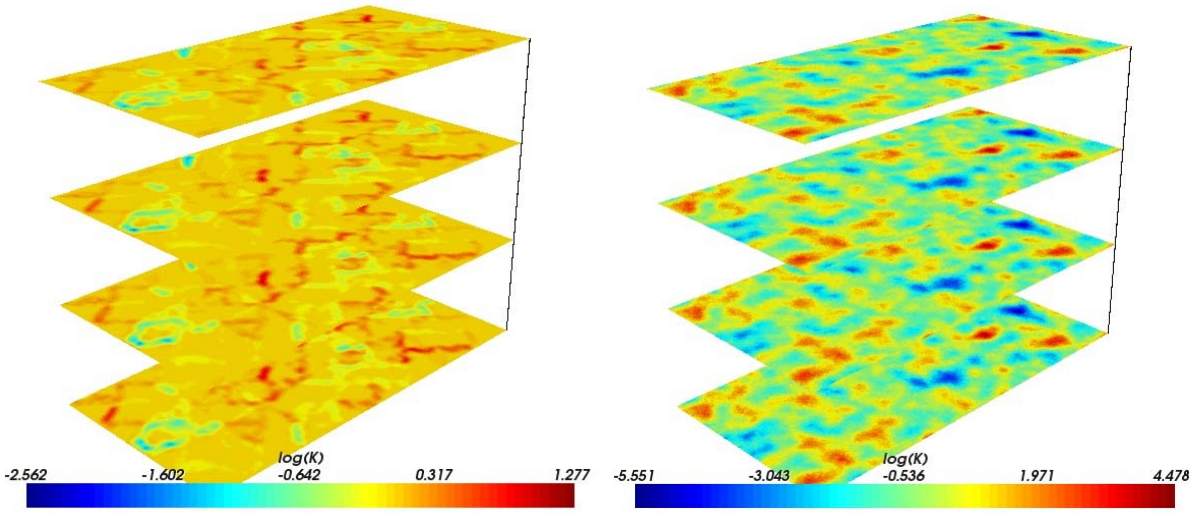

a) Derived-Initial Permeability Difference (Layer 5-8)

b) True-Initial Permeability Difference (Layer 5-8)

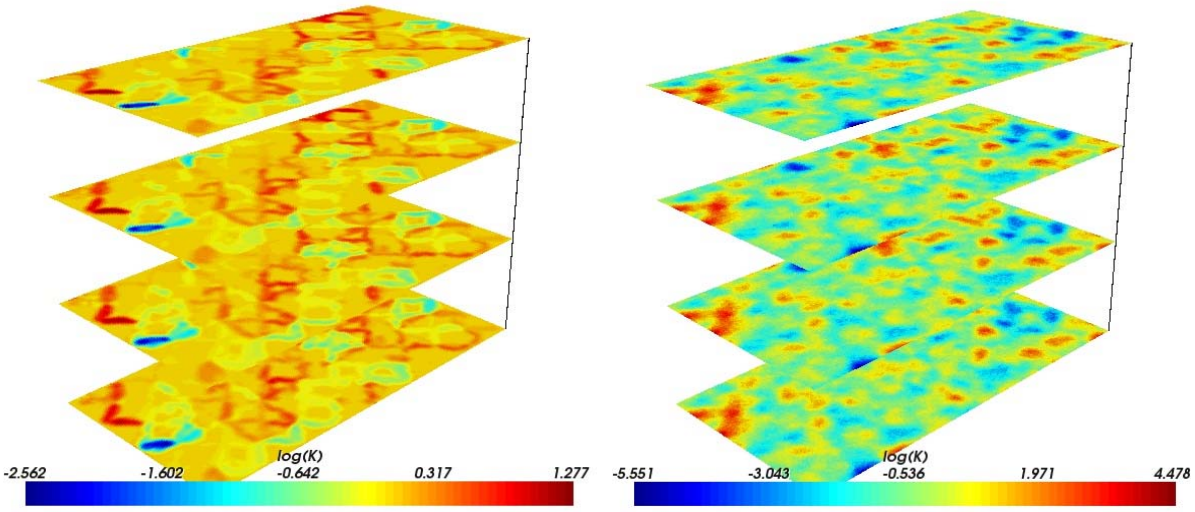

c) Derived-Initial Permeability Difference (Layer 29-32)

d) True-Initial Permeability Difference (Layer 29-32)

Fig. 17 – Case 2: Comparison of the "derived-initial" permeability difference and the "true-initial" permeability (MsMFEM [full]).